Cell Communication and Signaling

RESEARCH

Open Access

α-Klotho prevents diabetic retinopathy by reversing the senescence of macrophages

Qingbo Li[1,2,3], Peiyu Wang[1,2,3], Yi Gong[1,2,3], Manhong Xu[1,2,3], Manqiao Wang[1,2,3], Rong Luan[1,2,3], Juping Liu[1,2,3*], Xiaorong Li[1,2,3*] and Yan Shao[1,2,3,4*]

Abstract

Background Diabetic retinopathy (DR) is a common microvascular complication of diabetes mellitus (DM) and a significant cause of acquired blindness in the working-age population worldwide. Aging is considered as an important risk factor for DR development. Macrophages in aged mice bear typical M2 marker proteins but simultaneously express a pro-inflammatory factor profile. This may explain why the level of intraocular inflammation does not decrease during proliferative diabetic retinopathy (PDR) despite the occurrence of neovascularization and fibrosis (M2 activation). α-Klotho (KL) was originally discovered as a soluble anti-aging factor, which is mainly expressed in kidney tubular epithelium, choroid plexus in the brain and secreted in the blood. However, the role of KL in DR pathophysiology has not been previously reported.

Methods Type 1 (streptozotocin [STZ]-induced) and type 2 (a high-fat diet along with a low dose of STZ) diabetic mouse models were established and injected with or without KL adenovirus via the tail vein for 12 weeks. $Vldlr^{-/-}$ mice were injected intravitreally with or without soluble KL protein from P8 to P15. The retinal structure and function were analyzed by electroretinogram and optical coherence tomography. The neovascular lesions were analyzed by retinal flat mount and RPE flat mount. The senescence markers, macrophage morphology, and KL expression levels were detected by immunofluorescence staining. A cell model was constructed using RAW264.7 cells stimulated by 4-hydroxynonenal (4HNE) and transfected with or without KL adenovirus. The senescence-associated secretory phenotypes were detected by qRT-PCR. Senescence was detected by SA-β-Gal staining. Serum, aqueous humor, and vitreous humor KL levels of proliferative diabetic retinopathy (PDR) patients were measured by enzyme-linked immunosorbent assay. Quantitative proteomics and bioinformatics were applied to predict the change of proteins and biological function after overexpression of KL in macrophages. The effects of KL on the HECTD1 binding to IRS1 were analyzed by bioinformatics, molecular docking, and Western Blot.

Results Serum, aqueous humor, and vitreous humor KL levels were lower in patients with PDR than in those with cataracts. KL relieved the retinal structure damage, improved retina function, and inhibited retinal senescence in diabetic mice. KL administration attenuated the neovascular lesions in $VLDLR^{-/-}$ mice by decreasing the secretion of VEGFA and FGF2 from macrophages. KL also protected RAW264.7 cells from 4HNE-induced senescence. Additionally,

*Correspondence:
Juping Liu
tydljp@126.com
Xiaorong Li
lixiaorong@tmu.edu.cn
Yan Shao
sytmueh@163.com
Full list of author information is available at the end of the article

© The Author(s) 2024. **Open Access** This article is licensed under a Creative Commons Attribution-NonCommercial-NoDerivatives 4.0 International License, which permits any non-commercial use, sharing, distribution and reproduction in any medium or format, as long as you give appropriate credit to the original author(s) and the source, provide a link to the Creative Commons licence, and indicate if you modified the licensed material. You do not have permission under this licence to share adapted material derived from this article or parts of it. The images or other third party material in this article are included in the article's Creative Commons licence, unless indicated otherwise in a credit line to the material. If material is not included in the article's Creative Commons licence and your intended use is not permitted by statutory regulation or exceeds the permitted use, you will need to obtain permission directly from the copyright holder. To view a copy of this licence, visit http://creativecommons.org/licenses/by-nc-nd/4.0/.

it inhibited E3 ubiquitin ligase HECTD1 expression in both diabetic mouse peripheral blood mononuclear cells and 4HNE-treated RAW264.7 cells. KL inhibited HECTD1 binding to IRS1 and reduced the ubiquitination of IRS1.

Conclusions Macrophage aging is involved in DM-induced retinopathy. KL alleviates DM-induced retinal macrophage senescence by downregulating HECTD1 and decreasing IRS1 ubiquitination and degradation. Meanwhile, KL administration attenuated the neovascular lesions by altering the activation state of macrophages and decreasing the expression of VEGFA and FGF2.

Keywords Diabetic retinopathy, Aging, Macrophage, Ubiquitination

Introduction

Diabetes mellitus (DM) affects approximately 537 million adults worldwide, with projections indicating a rise to 643 million by 2030 and 783 million by 2045 [1]. Diabetic retinopathy (DR) is a common microvascular complication of diabetes and a significant cause of acquired blindness in the working-age population worldwide [2]. DR is clinically categorized into two stages according to disease severity: non-proliferative diabetic retinopathy (NPDR) and proliferative diabetic retinopathy (PDR). Current therapies can slow its progression but do not prevent or reverse it because of the multiple pathophysiological mechanisms. Therefore, novel therapeutic targets and strategies are required to improve DR treatment and prevention.

The incidence and prevalence of DR increase with age; therefore, aging is considered an important risk factor for DR development [3, 4]. Patients with DR experience have increased oxidative stress [5], which accelerates cellular aging through DNA damage [6]. Therefore, cellular senescence may be accelerated in patients with DR.

Macrophages play an important role in the pathogenesis of DR through retinal inflammation, neovascularization, and neurodegeneration [7, 8], including that of the classically activated state (M1) and the alternatively activated state (M2). M1 macrophages play a pro-inflammatory role by secreting pro-inflammatory cytokines such as interleukin-1β (IL-1β), IL-6, IL-12, IL-23, and TNF-α [9]. M2 macrophages play an anti-inflammatory role and promote tissue repair, remodeling, angiogenesis, and retain homeostasis by secreting large amounts of IL-10 and TGF-β [9]. However, the classical theory of macrophage polarization cannot explain that the upregulation of intraocular pro-inflammatory cytokines during PDR despite the occurrence of neovascularization and fibrosis (M2 activation). Recent studies have shown that macrophages in a mouse model of oxygen-induced proliferative retinopathy exhibit a unique phenotype with increased expression of both M1 and M2 markers [10]. Macrophage senescence is one of the numerous activation states that tissue-resident macrophages adopts in response to environmental stimuli [11]. Macrophages in aged mice bear typical M2 marker proteins but simultaneously express a pro-inflammatory factor profile [12, 13]. Therefore, senescent macrophages may be involved in the development of DR by promoting inflammation and angiogenesis.

α-Klotho (KL) was originally discovered as a soluble anti-aging factor [14], which is mainly expressed in kidney tubular epithelium, choroid plexus in the brain and secreted in the blood [15, 16]. It regulates phosphate and calcium metabolism, resists oxidative stress, and downregulates apoptosis, while exhibiting anti-inflammatory and anti-fibrotic functions [17]. Serum KL expression is significantly decreased in patients with DR and is negatively correlated with DR [18]. Consequently, increasing the serum KL level may have a significant improvement effect on DR.

In this study, we investigated the protective role of KL in DR and further explored the underlying mechanism. For the first time, we noted a close relationship between KL and macrophages in DR. Specifically, an increase in KL expression inhibited macrophage senescence via HECTD1/IRS1 pathway (Fig S1). Our report reveals new insight into the mechanism of DR, and might facilitate the development of future therapeutics to diminish the burden of this disease.

Materials and methods

Human sample collection

The participants were hospitalized patients with PDR, macular hole and cataract between November 2020 and November 2022 at the Tianjin Medical University Eye Hospital in Tianjin, China. PDR was based on the American Academy of Ophthalmology criteria (2019). Exclusion criteria were severe diabetic complications, severe and chronic infection symptoms, type 1 diabetes mellitus, liver and kidney dysfunction, malignant tumors, acute cardiovascular diseases, and patients with eye diseases other than cataracts or macular hole. Eventually, 45 patients with PDR, 29 with cataracts and 13 with macular hole were included. The anthropometric and biochemical characteristics of the participants are presented in Supplementary Table S1. Patients with cataracts underwent fundus photography, which confirmed no abnormalities

in the fundus. Informed consent was obtained from all participants prior to the survey, and the Research Ethics Committee of Tianjin Medical University Eye Hospital approved the study (2017KY-01).

Animals

Eight-week-old male C57BL/6 J mice (8 weeks old) were purchased from SiPiFu (Beijing, China). All mice were housed within ventilated cages in a specific pathogen-free room at a constant temperature (23 ± 2 °C) under a 12-h light–dark cycle at the Tianjin Medical University Eye Institute Laboratory Animal Center (Tianjin, China). The animals were categorized into four groups: (1) control for T1DM ($n=6$), (2) T1DM (streptozotocin [STZ]-induced) ($n=12$), (3) control for T2DM ($n=6$), and (4) T2DM (a high-fat diet [HFD] along with a low dose of STZ) ($n=12$). Mice were starved for 12 h before the experiment. The control mice of the T1DM group were induced by intraperitoneal injection of 0.1 M sodium citrate buffer (Solarbio, Beijing, China) for 5 days. In contrast, the T1DM mice were induced with STZ (40 mg/kg; Sigma-Aldrich, St. Louis, MO, USA) for 5 days. T2DM group's control mice were given a normal diet (10 kcal% fat, D12450J, Research Diets, Keaoxieli, Beijing, China) for 14 days before being starved and injected with 0.1 M sodium citrate buffer. T2DM mice were fed a high-fat diet (HFD) (60 kcal% fat, D12492, Research Diets, SaiNo, Jilin, China) for 14 days and were then induced with a single dose of STZ (85 mg/kg), followed by maintaining on a HFD. Subsequent blood glucose levels were measured by expressing a small amount of blood from the lateral tail vein after puncture with a 22-gauge needle and analyzing the sample using a blood glucose meter (ACCU-CHEK; Roche, Basel, Switzerland). Mice with plasma glucose levels > 16.7 mmol/L were considered diabetic.

Adenovirus (Ad) vectors containing a null transgene (Ad-null) or a KL transgene (Ad-KL) were purchased from Scilia (Beijing, China). The diabetic group was further categorized into four subgroups: T1DM + Ad-null ($n=6$), T1DM + Ad-KL ($n=6$), T2DM + Ad-null ($n=6$), and T2DM + Ad-KL ($n=6$). Diabetic mice receiving KL treatment were injected with 2.5×10^9 plaque-forming units of Ad-KL via the tail vein, and Ad-null was injected as a control. The adenoviral transfer was repeated monthly after the first dose. The mice were euthanized 12 weeks after the first adenovirus injection (Fig S2).

Vldlr$^{-/-}$ mice were provided by Jackson Laboratory. The mouse pups were treated with an intravitreal injection of soluble KL protein (3 pmol/L) or PBS from P8 to P15. At P16, neovascular lesions were quantified.

The use of animals in the experimental protocol was approved by the Tianjin Medical University Eye Institute Laboratory Animal Center (TJYY20231202894). All animal experiments were performed in accordance with the ARVO Statement for the Use of Animals in Ophthalmic and Vision Research.

Cell culture

RAW264.7 lineage cells were cultivated with DMEM medium (Gibco, Gaithersburg, MD) supplemented with 10% fetal bovine serum (Gibco), 100 IU/mL penicillin and 100 mg/mL streptomycin (Beyotime, Shanghai, China) under 37 °C in a 5% carbon dioxide environment in a humid incubating device. The cells were cultured in 6-well plates and transfected with Ad-KL. Cells (1×10^6 cells/well) were infected with the virus at an MOI of 100. After the cells were treated with the virus for 24 h, 4-hydroxynonenal (4HNE) (Cayman Chemical, Ann Arbor, MI), 10 μmol/L was administrated for 72 h, and the cells were harvested.

Wound healing

RAW264.7 cells (1×10^6 cells / well) were seeded in a 6-well culture plate for 24 h, until they reached a confluence of 90%. Scratched wound lines were created using a 10 μL micropipette tip. Cells were treated for 24 h in serum-free medium with or without 50 ng/mL soluble KL protein (Cloud-Clone Corp.) and cultured for 24 h. The Scratched wound lines were examined using an Olympus microscope (DP73; Olympus, Tokyo, Japan), and calculated using the ImageJ software.

SA-β-Gal staining

Staining for SA-β-gal activity was performed according to the manufacturer's instructions (C0602; Beyotime, Shanghai, China). Briefly, cells and retinal sections were fixed in a fixative solution, and stained in a staining working solution containing X-gal for 24 h at 37 °C. Imaging was observed using an Olympus microscope, where senescent cells were stained blue.

Isolation of mouse peripheral blood mononuclear Cells (PBMCs)

Blood samples were collected by enucleation of eyeballs, and then PBMCs were isolated by a mouse peripheral blood mononuclear cells isolation kit (Tbdscience, Tianjin, China). Briefly, the mononuclear cell layer was collected after density gradient centrifugation, washed three times with wash buffer, and centrifuged at 250 g for 10 min at room temperature to obtain mononuclear cell precipitates. The resulting mononuclear cell precipitate was used for protein extraction.

3D structure preparation and molecular docking of HECTD1 and IRS1

Molecular docking of HECTD1 and IRS1 crystal structures was performed to investigate protein–protein interaction (PPI). The solved crystal structures of the HECTD1 solution NMR structure (PDB ID 2LC3) and the IRS1 PTB domain (PDB ID 1IRS) were obtained from the UniProt database (https://www.uniprot.org/). Protein–protein molecular docking of HECTD1 and IRS1 was performed using ClusPro 2.0. Finally, images of the interactions were prepared using PyMOL 2.5.

Bioinformatics analyses

The dataset GSE26168 was downloaded from the Gene Expression Omnibus (GEO) (https://www.ncbi.nlm.nih.gov/geo/). Samples from nine T2DM samples and eight healthy controls were analyzed. GEO2R was used to explore differentially expressed genes (DEGs) between T2DM and normal blood samples, and heat maps were generated using ggplot2. Statistically significant DEGs were defined as $|\log FC| \geq 1$, and a P-value < 0.05 was the cut-off criterion. Senescence-related genes obtained from the Aging Atlas were 500 (https://ngdc.cncb.ac.cn/aging/age_related_genes). The PPI network of differentially expressed senescence-related genes was examined using the Search Tool for the Retrieval of Interacting Genes (STRING) database (https://string-db.org/). The PPI network was visualized and constructed using Cytoscape v3.8.2 software. Finally, 10 hub genes were screened by the cytoHubba plugin.

Data independent acquisition (DIA) quantitative proteomics

Six samples consisting of three biological replicates of two groups, Ad-null-transfected RAW264.7 cells, were prepared. Proteins were extracted using lysis buffer containing 8 mol/L urea, 50 mmol/L NH4HCO3, and 0.2% SDS, followed by 5 min of ultrasonication on ice. The lysate was centrifuged at 14,000 × g for 10 min at 4 °C, and the supernatant was moved to a clean tube. The protein concentration was measured using the bicinchoninic acid method, and 100 μg of protein was extracted from each sample. The samples were further reduced with 10 mM DTT for 1 h, then alkylated with 40 mM IAA for 1 h at room temperature in the dark. The protein was digested with trypsin at a ratio of 1:40 for 12–16 h at 37 °C. Samples were centrifuged at 14,000 rcf for 20 min at 4 °C, and digested peptides were collected using 50 μL NH4HCO3 in three subsequent elution steps. Formic acid (1%, 7.5 μL) was added to the mixed digested peptides to stop digestion, and samples were dried under vacuum at 60 °C for 45 min. The peptides were resuspended in 12 μL of 0.1% formic acid. Peptide concentration was measured using a Nanodrop spectrophotometer (Thermo Scientific, Basel, Switzerland) at an absorbance of 280 nm; 4 μg peptides were separated on a 30 min LC gradient using a Trap column (AB SCIEX, 10 × 0.3 mm, 5 μm 120 A C18 particles) and injected into Triple TOF 6600 (SCIEX, Framingham, MA, USA) mass spectrometer. The DIA acquisition scheme consisted of 96 variable windows ranging from 100 to 1500 m/z. Raw data from DIA quantitative proteomics were analyzed using Spectronaut 15 and searched against the UniProt Macaca mulatta database (https://www.uniprot.org/proteomes/UP000006718). A confidently identified protein requires at least one unique peptide with an FDR < 1%. We defined proteins with $|\log FC| \geq 1.5$ and a P-value < 0.05 as differentially expressed proteins (DEPs). Heatmaps were generated using the "pheatmap" package in R, and volcano plots using "ggplot2." Gene ontology (GO) pathways were searched using the "clusterProfiler" package in R.

Query for E3-HECTD1 Interactions in UbiBrowser 2.0

UbiBrowser 2.0 (http://ubibrowser.bio-it.cn/ubibrowser_v3/) is a comprehensive database that predicts proteome-wide E3-substrate networks based on a naïve Bayesian classifier and combines various types of heterogeneous biological evidence. It currently contains 4068 known E3-substrate interactions in 38 organisms. This was used to predict the potential substrates of HECTD1.

Measurement of KL level by enzyme-linked immunosorbent assay (ELISA)

Human KL ELISA kit was obtained from ImmunoBiological Laboratories (Takasaki, Japan). The ELISA was performed according to the manufacturer's instructions. Briefly, 100 μL of EIA buffer, prepared standard and serum and aqueous humor samples were added to appropriate wells. The resulting plate was incubated for 60 min at room temperature with plate lid and subsequently washed four times with wash buffer. After removing all liquid completely, 100 μL of labeled antibody was added to each well. The resulting plate was incubated for 30 min at room temperature with a plate lid and subsequently washed four times with wash buffer. After washing the wells, 100 μL of TMB solution was added and incubated for 30 min at room temperature. Finally, the reaction was stopped by adding 100 μL stop solution, and the signal was measured at 450 nm.

RNA interference analysis

A small interfering RNA of HECTD1 (HECTD1-siRNA) was purchased from GenePharma (Shanghai, China). RAW264.7 cells were seeded in a 6-well plate with DMEM for 12 h before the transfection. The cells were then transfected with HECTD1-siRNA and negative

control siRNA (NC-siRNA) for 72 h using Lipofectamine 2000 (Thermo Fisher Scientific, MA, USA) in Opti-MEM medium (Thermo Fisher Scientific, MA, USA). The sequences are as follows:

HECTD1 siRNA: F: 5′-GCCAUCUACUUCAAG UCAATT-3′; R: 5′-UUGACUUGAAGUAGAUGG CTT -3′.
Negative control: F: 5′-UUCUCCGAACGUGUC ACGUTT-3′; R: 5′- ACGUGACACGUUCGGAGA ATT -3′.

Western blot analysis

Cells were sonicated using radioimmunoprecipitation assay (RIPA) lysis buffer (Solarbio, Beijing, China), and then centrifuged at 14,000 rpm for 30 min at 4 °C. Protein concentrations in the supernatants were detected using the bicinchoninic acid (BCA) protein assay kit (Solarbio, Beijing, China). Next, 20 μg of protein samples were separated by SDS-PAGE and transferred to polyvinylidene fluoride; membranes were blocked with a blocking buffer (Epizyme, Shanghai, China) for 20 min, and then incubated with the primary antibodies overnight at 4 °C. Membranes were washed and incubated with either HRP-conjugated goat anti-rabbit or anti-mouse IgG for 2 h at room temperature. The antibodies used in this study are listed in Supplementary Table S2. Signals were developed using enhanced chemiluminescence substrate (Amersham, Buckinghamshire, U.K.) and visualized using autoradiography (Tanon, Shanghai, China). The gray density of the bands was performed using ImageJ software (NIH, Bethesda, MD, USA).

Immunoprecipitation and ubiquitylation assays

HECTD1 knockout RAW264.7 cells were lysed and combined with 6 μg of anti-IRS1 (proteintech, Wuhan, China) per sample at 4 °C overnight. Next, the antigen sample/antibody mixture was added to the tube containing 25 μL Pierce Protein A/G Magnetic Beads (Thermo Fisher Scientific, Waltham, MA, USA) at room temperature for 1 h with mixing. The beads were incubated with 100μL 1X lane marker sample buffer at 100°C for 10 min and then Western blotting with anti-ubiquitin (PTM BIO, Hangzhou, China) was performed.

Immunofluorescence assay

The cell slides and retinal flat mounts were fixed with 4% paraformaldehyde for 20 min. Cell and tissue slides were blocked with 0.2% bovine serum albumin (BSA) (Beyotime, Shanghai, China) and 5% goat serum (Gibco; Thermo Fisher Scientific, Massachusetts) in 0.3% Triton X-100 (Solarbio, Beijing, China) for 30 min at 4 °C. The diluent primary antibody was incubated overnight at 4 °C. After a washing step, the slides were incubated with diluent secondary antibodies conjugated to Alexa Fluor 488/594 for 2 h at room temperature. After counterstaining with DAPI, the slides were mounted in an antifade mounting medium (Solarbio, Beijing, China) and observed under a confocal microscope (Zeiss, Germany). The primary antibodies used are listed in Supplementary Table S2.

Quantitative real-time polymerase chain reaction (qRT-PCR)

Total mRNA was isolated from RAW264.7 using an RNA extraction kit (EZBioscience, US). The concentration of total RNA was measured by a NanoDrop 2000 spectrophotometer (Thermo Fisher Scientific, Waltham, USA, MA) and was reverse-transcribed into cDNA using the color reverse transcription reagents (EZBioscience, US). Gene-specific primers were designed using the Primer-BLAST (Supplementary Table S3). Each qPCR reaction was performed using 2μL of cDNA and 1.5 μL of each primer in 5 μL of 2X Color SYBR Green Master Mix (EZ Bioscience, US). The cycling conditions were as follows: 5 min at 95 °C, 40 cycles for 10 s at 95 °C, and 30 s at 60 °C. The SYBR Green fluorescence signal was measured

(See figure on next page.)

Fig. 1 The aging of macrophages plays a role in DM-induced retinopathy. **A** SA-β-gal staining and immunofluorescence of anti-P53 (red) antibody in the retina; scale bar = 20 μm ($n = 3$). **B** The fluorescence intensity of P53 was quantified and is displayed in the bar graph. **C** Western blotting measured the protein expression level of P21 and P16 in the retina of T2DM mice compared to the Normal group ($n = 3$). **D**, **E** Bar graph showing quantification of P21 and P16 expression in western blot (n = 3). **F** Immunofluorescence of anti-F4/80 (red) antibody in the retina; scale bar = 20 μm ($n = 3$). **G** SA-β-gal staining and immunofluorescence of anti-P53 (green) antibody in RAW264.7 cells; scale bar = 50 μm/20 μm ($n = 3$). **H** The fluorescence intensity of P53 was quantified and is displayed in the bar graph ($n = 3$). **I** Western blotting measured the protein expression level of P21 and P16 in 4HNE-induced RAW264.7 cells compared to the control group ($n = 3$). **J**, **K** Bar graph showing quantification of P21 and P16 expression in western blot (n = 3). (L) Quantification of SASP mRNA expression in RAW264.7 cells ($n = 6$). β-actin was used as control. (M) Immunofluorescence of anti-Ki67 (green) antibody in RAW264.7 cells; scale bar = 20 μm ($n = 3$). (N) Proportions of Ki67 positive cells in different groups. (O) Western blotting measured the protein expression level of P53, P21, and P16 in the mouse PBMCs ($n = 3$). (P, Q, R) Bar graph showing quantification of P53, P21, and P16 expression ($n = 3$). Data represent the mean ± SEM. $*p < 0.05$, $**p < 0.01$, $***p < 0.001$, $****p < 0.0001$, by independent samples t-test

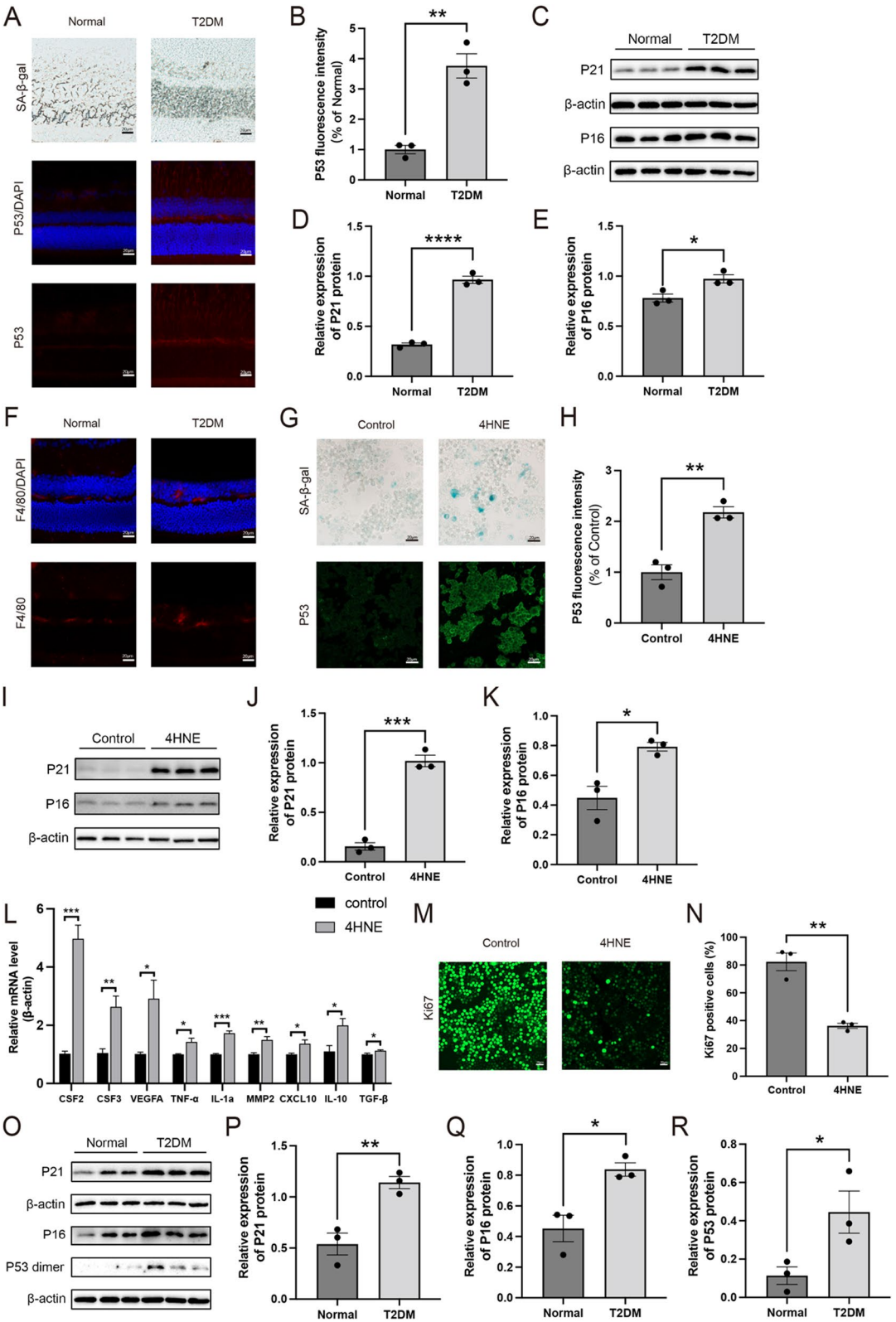

Fig. 1 (See legend on previous page.)

at the end of each cycle using a LightCycler 480 II (Roche, Basel, Switzerland).

Electroretinography (ERG)

Mice were anesthetized with 5% chloral hydrate after at least 12 h of dark adjustment. Their pupils were fully dilated with tropicamide, and topical anesthesia was administered before recording began. Electrical responses were recorded using a forehead reference electrode and a ground electrode in the tail. Ganzfeld stimuli were delivered using Phoenix Micron IV (Phoenix Technologies, Beaverton, USA). Dark-adapted ERGs (1.0 cd. s/m^2 flash stimuli) were recorded.

Optical coherence tomography (OCT)

The thickness of each layer of mouse retina was measured using a Spectralis OCT (Heidelberg, Germany). Animals were anesthetized with 5% chloral hydrate. During sedation, tropicamide eye drops were administered to dilate the pupil. OCT images were acquired using 768 A scans, 30 B scans, and a 30-degree OCT field. Total retinal thickness and thickness of separate retinal layers were analyzed using the device's internal software (Heidelberg Eye Explorer Software).

Statistical analysis

All experiments were repeated at least thrice. All statistical analyses were performed with the Prism software (GraphPad, San Diego, CA, USA). Data are presented as standard error of the mean (SEM). All groups were normalized to the control group unless otherwise stated, and statistical analysis was carried out with unpaired Student's t-tests, analysis of variance (ANOVA), and chi-square tests. Results were considered significant when $P < 0.05$.

Results

Senescence of macrophages is involved in DM-induced retinopathy

Aging cells were increased in the retinas of the DM group, as shown by staining with SA-β-gal, which is indicator of cellular senescence (Fig. 1A). The protein expression levels of aging-associated proteins including P53, P21, and P16 were upregulated significantly in the retina of DM group (Figs. 1A-E). In the Normal group, retinal immunolabeling with the marker F4/80 showed ramified macrophages in the outer plexiform layer (Fig. 1F). In contrast to the normal group, in which ramified macrophages were absent, retinal sections from the DM group showed the migration of many macrophages to the inner nuclear layer. The cells in this region were amoeboid (Fig. 1F). Thus, we hypothesized that the changes in macrophage morphology were because of DM-induced macrophage senescence in the retinas of diabetic mice. Oxidative stress mediated by 4HNE is the important pathophysiological mechanism of the development of DM [19, 20]. We established a DM cell model utilizing the 4HNE to verify whether DM induces macrophage senescence. We detected the expression of several senescence markers, including SA-β-gal, senescence-associated secretory phenotype (SASP), Ki67, and expression levels of P53, P21, and P16, after treatment with 10 μM 4HNE at 72-h intervals. The results of the SA-β-gal demonstrated that RAW264.7 cells became more senescent after treatment (Figs. 1G). P53, P21, and P16 protein levels and SASP mRNA levels were all increased significantly in 4HNE treatment groups (Figs. 1G-L), whereas the percentage of Ki67-positive cells were clearly reduced (Figs. 1M, N). Additionally, P53, P21, and P16 protein levels were also upregulated in PBMCs isolated from diabetic mice compared to the control group (Figs. 1O-R). These data suggest that senescent macrophages play a role in DM-induced retinopathy.

(See figure on next page.)

Fig. 2 KL expression was decreased in DM group. **A** Comparison of serum KL levels between cataract patients (Control group; $n = 15$) and PDR patients (PDR group; $n = 16$). Data are represented as box plots. **B** Comparison of aqueous humor KL levels between cataract patients (Control group; $n = 14$) and PDR patients (PDR group; $n = 14$). Data are represented as box plots. **C** Comparison of vitreous humor KL levels between macular hole patients (Control group; $n = 13$) and PDR patients (PDR group; $n = 15$). Data are represented as box plots. (D) Immunofluorescence of anti-KL (green) antibody in the retina of diabetic mice as compared with their controls; scale bar = 20 μm ($n = 3$). **E** The fluorescence intensity of KL was quantified and is displayed in the bar graph. (F) Western blotting measured the protein expression level of KL in the retina of diabetic mice compared to the control group ($n = 3$). (G) Bar graph showing quantification of KL expression in western blot ($n = 3$). **H**, **I** The qRT-PCR analysis of KL mRNA levels in RAW264.7 cells after the treatment ($n = 6$). β-actin was used as a loading control. **J** Western blotting measured the protein expression level of KL in 4HNE-induced RAW264.7 cells compared to the control group ($n = 3$). (K) Bar graph showing quantification of KL expression in western blot ($n = 3$). **L** The migration of RAW264.7 cells was analyzed using the cell scratch assay, and cells were photographed after 50 ng/ml KL treatment for 24 h ($n = 3$). (M) The quantification for cell scratch assay. Data represent the mean ± SEM. $*p < 0.05$, $**p < 0.01$, by independent samples t-test and one-way ANOVA

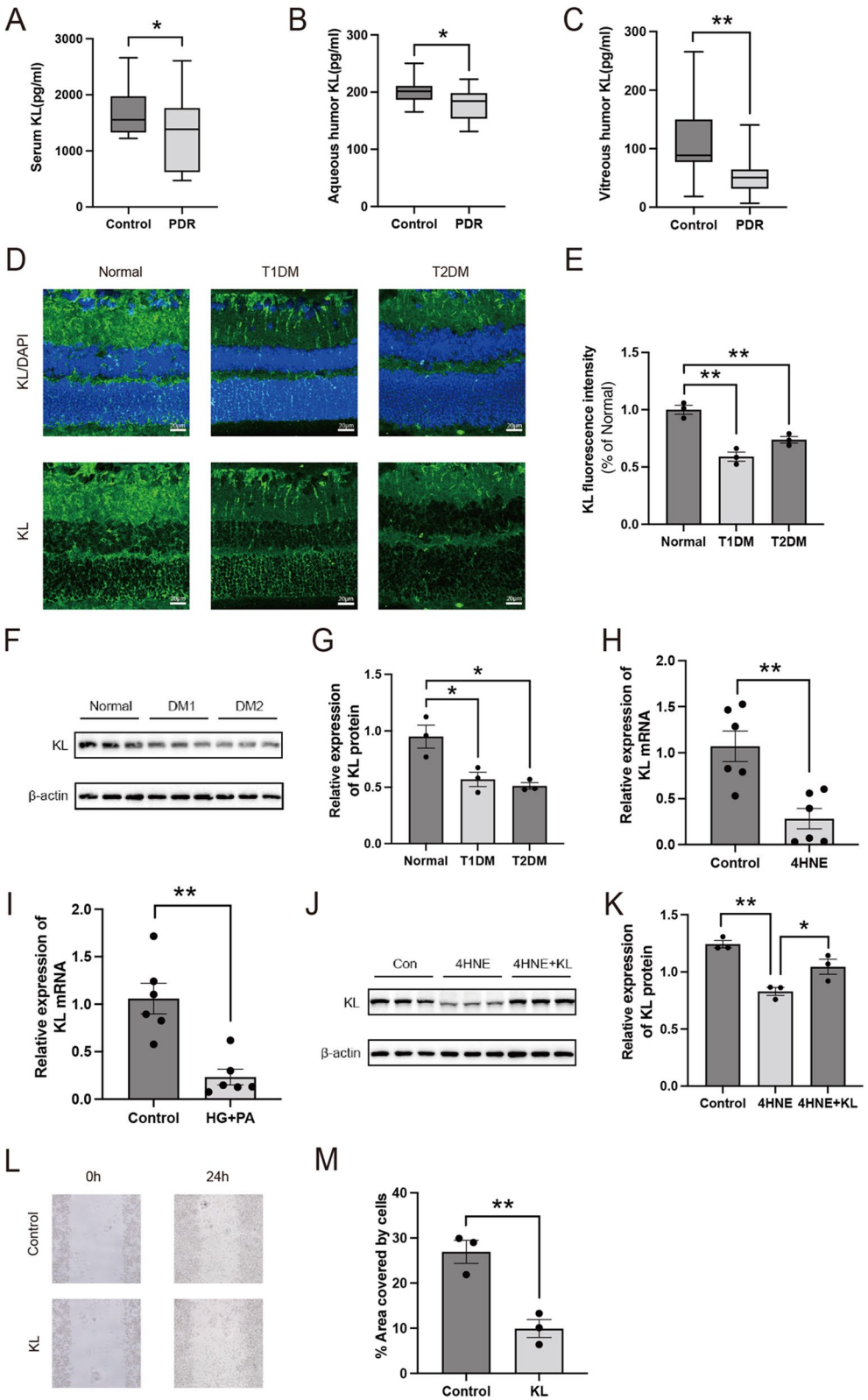

Fig. 2 (See legend on previous page.)

Influence of DM on KL level

As shown in Fig. 2A, the serum KL level was lower in the PDR group (1288.69 pg/mL, IQR 648.90–1716.69 pg/mL) than in the Control group (1717.20 pg/mL, IQR 1347.79–1975.60 pg/mL; $P=0.047$). The aqueous humor KL level was lower in the PDR group (177.56 pg/mL, IQR 156.49–192.33 pg/mL) than in the Control group (201.92 pg/mL, IQR 187.54–208.38 pg/mL; $P=0.022$; Fig. 2B). Furthermore, the vitreous humor KL level was also lower in the PDR group (51.81 pg/mL, IQR 33.97–64.58 pg/mL) than in the Control group (113.67 pg/mL, IQR 79.57–137.92 pg/mL; $P=0.007$; Fig. 2C). Similarly, KL expression decreased in the retinas of diabetic mice (Figs. 2D-G). RAW264.7 cells were examined at 72-h intervals after 10 μM 4HNE or 25 mM glucose and 300 μM palmitic acid (PA) exposure to further assess the expression of KL in macrophages. KL expression was lower than in the control group after treatment (Figs. 2H-K). In addition, we conducted scratch-healing experiments to investigate the effect of KL on the migration of RAW264.7 cells. The results showed that scratch healing after incubation with 50 ng/ml KL for 24 h was much worse than in the control group in RAW264.7 cells (Figs. 2L, M).

KL treatment protects the retina from DM-induced degeneration

Next, we investigated whether targeting retinal macrophages with KL improved DR progression. OCT was performed to evaluate the structural changes in the retinas of diabetic mice (Figs. 3A, B). Volume scans revealed severe thinning of the retina in diabetic mice, which was reversed in the KL-treated groups (Figs. 3C, E). Quantification of retinal thickness demonstrated that the ganglion cell layer was significantly reduced in the T2DM group, and the ganglion cell, retinal pigment epithelium (RPE), and photoreceptor layers were significantly reduced in the T1DM group (Figs. 3D, F–H). The intravenous injection of Ad-KL rescues the changes (Figs. 3D, F–H). We performed ERG to detect electrophysiological changes in the retina (F igs. 3I, J). The mean a-wave and b-wave amplitudes in diabetic mice were significantly smaller than in the Normal group (Figs. 3K-N). Interestingly, KL reversed the reduction in the a- and b-waves associated with DM (Figs. 3K-N). These data clearly demonstrate the strong protective effect of KL on retinal structure and function under diabetic conditions.

KL administration attenuated the neovascular lesions by altering the activation state of macrophages

The absence of the very low-density lipoprotein receptor (VLDLR) is associated with retinal angiomatous proliferation and neovascularization [21, 22]. In $Vldlr^{-/-}$ mice, abnormal blood vessels extend toward photoreceptor outer segments [22]. We found that $Vldlr^{-/-}$ mice showed an obvious increase of vascular leakage and pathologic retinal neovascularization with macrophage activation at P15 compared with Normal group (Fig. 4A). We administered soluble KL protein intravitreally at 3 pmol/L daily from P8 to P15 to $Vldlr^{-/-}$ mice to assess whether KL protects against DM-induced pathologic neovessel growth. Our results indicated that KL reduced the vascular leakage and pathologic retinal neovascularization in the $Vldlr^{-/-}$ mice (Figs. 4B-D). Meanwhile, we observed the accumulation of macrophages at the neovascularization in the RPE layer (Fig. 4E). Under pathological conditions, recruited macrophages erode the RPE and facilitate neovascularization growth [23]. The growth factors VEGFA and FGF2 show a combined effect on both angiogenesis of blood vessels [24]. Therefore, we determined the levels of these factors in RAW264.7 cells transfected with KL. According to the WB results, 4HNE significantly upregulated the expression of VEGFA and FGF2 (F igs. 4F-I). Changes in VEGFA and FGF2 expression were reversed after KL overexpression (F igs. 4F-I). We demonstrated that alternation of macrophages activation status and down-regulation of VEGF and FGF2 by KL resulted in a reduced neovascularization.

KL recovers DM-induced retinal macrophage senescence

We examined the retinas of diabetic mice to confirm the role of KL in DM-induced retinal senescence. In tail vein-injected diabetic mice (Ad-KL group), SA-β-gal-positive cell counts were successfully down-regulated compared

(See figure on next page.)

Fig. 3 KL prevents DM-induced retinal degeneration. **A** Representative OCT images of the Normal group, T2DM group and T2DM + KL group are presented. A definition of the retinal layers is shown on the right of the panel. **B** Representative OCT images of the Normal group, T1DM group and T1DM + KL group are presented. **C**, **D** The total retinal and ganglion cell layer thickness was obtained from OCT in the Normal group, T2DM group and T2DM + KL group ($n=6$). (E–H) Thickness of the total retinal, ganglion cell layer, RPE layer and photoreceptor layer obtained from OCT in the Normal group, T1DM group and T1DM + KL group. **I** Representative diagrams of a-wave and b-wave from the Normal group, T2DM group and T2DM + KL group. **J** Representative diagrams of a-wave and b-wave from the Normal group, T1DM group and T1DM + KL group. **K**, **L** Amplitudes of a-waves and b-waves in the ERG waveform were analyzed by histogram from the Normal group, T2DM group and T2DM + KL group ($n=6$). (M, N) Amplitudes of a-waves and b-waves in the ERG waveform were analyzed by histogram from the Normal group, T1DM group and T1DM + KL group ($n=6$). Data represent the mean ± SEM. $*p<0.05$, $**p<0.01$, $***p<0.001$, $****p<0.0001$, by one-way ANOVA

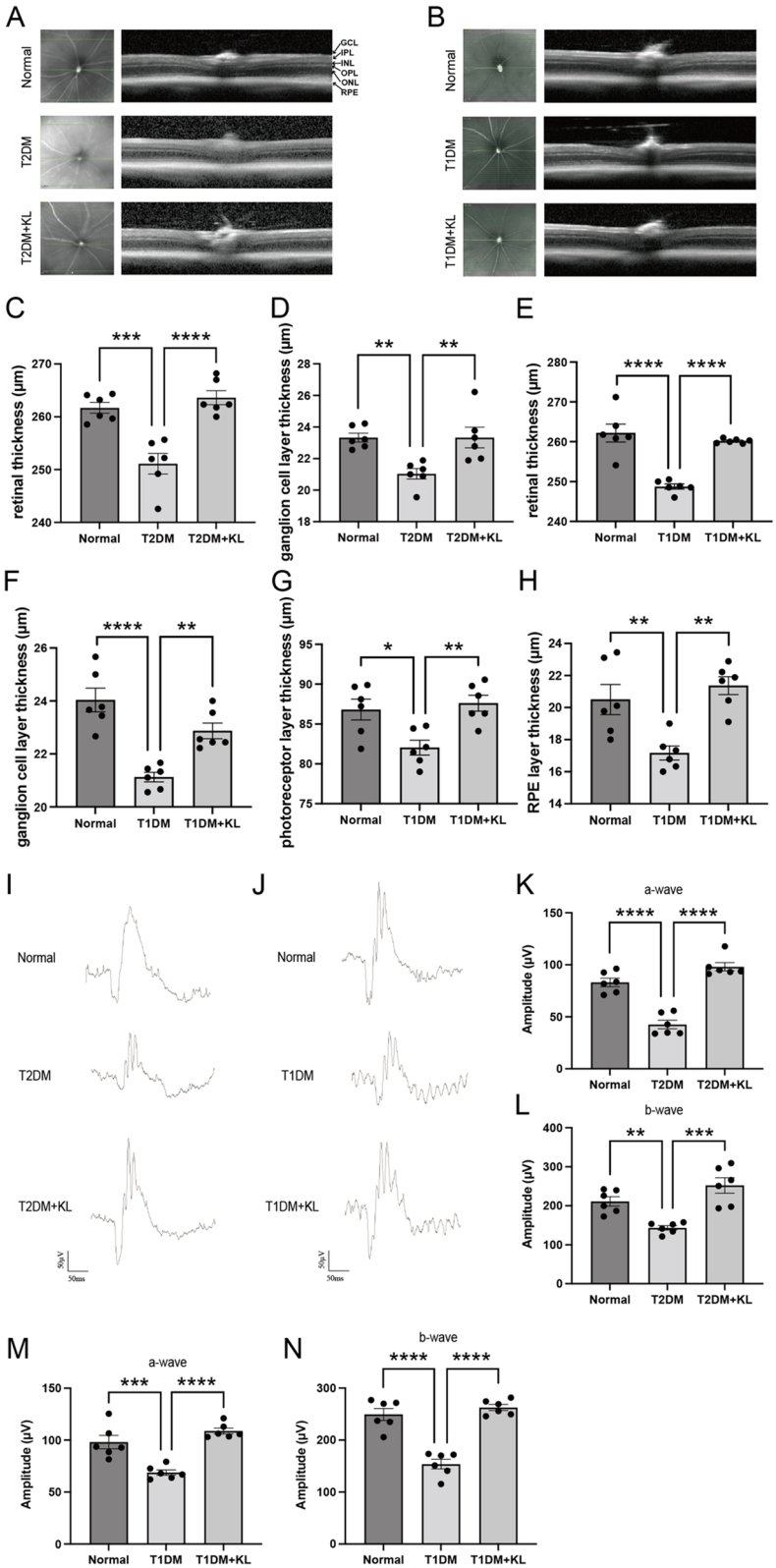

Fig. 3 (See legend on previous page.)

with those in mice that received the control virus (Ad-null group) (Figs. 5A). In addition, the protein expression levels of P53, P21, and P16 in retina were all down-regulated in Ad-KL group (Figs. 5A-E). Treatment with KL reversed the morphology of macrophages. It prevented their migration to the inner nuclear layer (Fig. 5F). In addition, RAW264.7 cells were transfected with Ad-KL or Ad-null to clarify whether KL reverses 4HNE-induced macrophage senescence. SA-β-gal staining results illustrated that KL significantly reduced SA-β-gal-positive cell counts in RAW264.7 cells (Fig. 5G). Similarly, KL overexpression inhibited P53, P21, and P16 protein levels and SASP mRNA levels in RAW264.7 cells (Figs. 5G-L). Next, we examined Ki67 in RAW264.7 cells using immunofluorescence. Upregulation of Ki67 expression by KL overexpression was also observed (Figs. 5M, N). Additionally, P53, P21, and P16 protein levels were also down-regulated in PBMCs isolated from Ad-KL group compared to the Ad-null group (Figs. 5O-R). These results showed that KL reversed macrophage senescence in the retina of diabetic mice.

Prediction of the mechanism of anti- senescence activity of KL

We explored the mechanism by which KL regulates macrophage senescence. RAW264.7 macrophages transfected with Ad-KL were used for proteomic analysis. Compared to the control group, macrophages transfected with ADV-KL exhibited 203 DEPs (92 down-regulated proteins and 111 upregulated proteins) (Figs. 6A, B). According to GO analyses, in combination with the biological characteristics of the ubiquitin–proteasome, ubiquitination may participate in the role of KL in reversing macrophage senescence (Fig. 6C). We further studied DEPs and found that the expression of the E3 ubiquitin ligase HECTD1 was decreased, which might be a key molecule involved in the modulation of macrophage senescence by KL (Fig. 6B). We then predicted the potential substrates of HECTD1 using the Ubibrowser website (Fig. 6D). We downloaded the expression profiles using the array dataset GSE26168 from the GEO database. We selected blood samples from eight non-diabetic individuals and nine patients with T2DM. Based on the threshold mentioned above ($|\log FC| \geq 1$ and $P < 0.05$), 851 DEGs, including 429 upregulated and 422 down-regulated DEGs, were filtered using GEO2R (Fig. 6E). In total, 500 senescence-related genes were obtained from Aging Atlas. We then generated Venn diagrams to identify overlapping DEGs (Fig. 6F). We used the STRING database to construct a PPI network toward a deeper understanding of the interactions between the differentially expressed senescence-related genes (Fig. 6G). The 10 hub genes with the highest values were screened using Cytoscape (v3.8.2) (Fig. 6H). Among these, IRS1, a potential substrate of HECTD1, was down-regulated. Thus, we hypothesized that KL alleviates DM-induced retinal macrophage senescence by downregulating HECTD1 and decreasing IRS1 ubiquitination and degradation.

KL alleviates macrophage senescence by downregulating HECTD1 expression

To demonstrate the interaction of HECTD1 and IRS1, the protein–protein docking tool ClusPro 2.0 was used for the docking study of the HECTD1 solution NMR structure (PDB ID 2LC3) and IRS1 PTB domain (PDB ID 1IRS) (Fig. 7A). Lipofectamine 2000 was used to transfect HECTD1-siRNA into RAW264.7 cells. We further discovered that the knockout of HECTD1 significantly increased the protein levels of IRS1 which in turn increased the expression of proteins associated with the PI3K-Akt signaling pathway. (Figs. 7B-E). Meanwhile, we analyzed whether HECTD1 regulates the IRS1 ubiquitination. Silencing HECTD1 decreased IRS1 ubiquitination (Fig. 7F). Then we determined the levels of these factors in cells transfected with KL to examine whether HECTD1 and IRS1 were involved in KL-mediated regulation of senescence in RAW264.7. According to the WB results, 4HNE significantly upregulated the expression of HECTD1 and down-regulated the expression of IRS1 (Figs. 7G-J). Changes in HECTD1 and IRS1 expression were reversed after KL overexpression (Figs. 7G-J). We also isolated PBMCs from mouse blood samples and examined the expression of HECTD1 and IRS1. These results are consistent with RAW264.7 cells the in vitro (Figs. 7K, L). These results indicate that KL regulates

(See figure on next page.)

Fig. 4 KL administration attenuated the neovascular lesions by altering the activation state of macrophages. **A** The representative image of the retinal flat mount with IB4 (red) and F4/80 (F4/80) in different magnifications; scale bar = 500/20 μm ($n = 3$). **B** IB4 and CD34 staining showed reduced neovascularization and vascular leakage in $Vldlr^{-/-}$ retinas from mice with KL administration; scale bar = 500 μm ($n = 3$). **C** The representative image of the RPE flat mount with IB4 (red) and CD34 (green); scale bar = 5 μm ($n = 3$). **D** 3D reconstruction of retinal neovessels extending from the outer plexiform layer (OPL) towards the RPE. Soluble KL protein decreased retinal neovessel extension towards RPE seen with IB4 (red) and CD34 (green) stained vessels. **E** The representative image of the RPE flat mount with IB4 (red) and F4/80 (green); scale bar = 20 μm ($n = 3$). (F-I) RAW264.7 cells were further treated with 4HNE after transfection with ADV-GFP or ADV-KL. The expression of VEGFA and FGF2 in cells was investigated and quantified ($n = 3$). Data represent the mean ± SEM. $*p < 0.05$, $**p < 0.01$, by independent samples t-test and one-way ANOVA

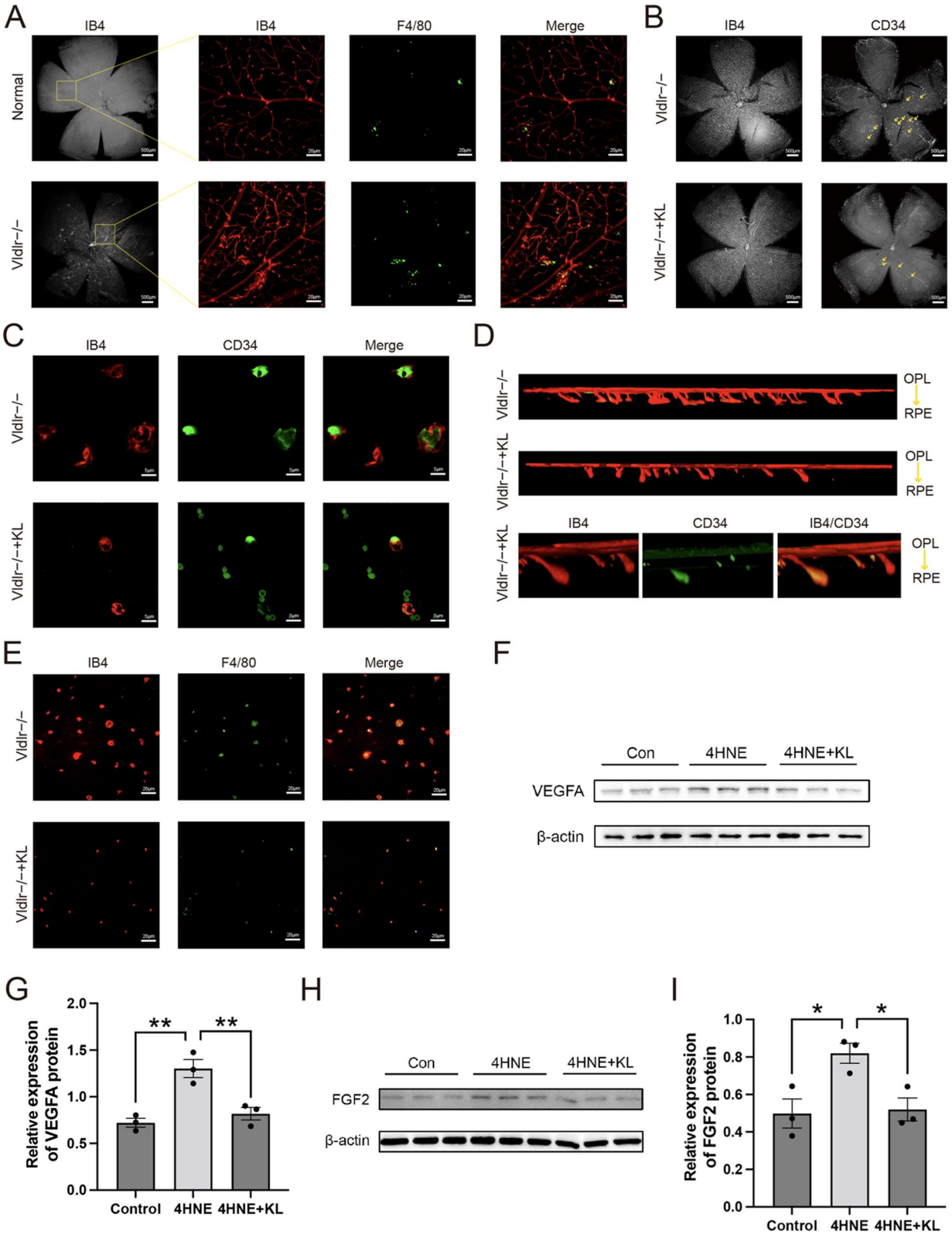

Fig. 4 (See legend on previous page.)

HECTD1 and IRS1 in macrophages, which play a critical role in the KL-mediated regulation of senescence.

Discussion

DR has become the leading cause of blindness for adults in developed countries with the rapid increase in diabetes cases [25]. Recent studies have shown that multiple metabolic pathways are involved in developing DR and cellular senescence, including oxidative stress, endoplasmic reticulum stress, lipid metabolism and autophagy dysfunction [26–33]. This demonstrates a close relationship between DR and cellular senescence [4]. Here, we report for the first time, that senescent macrophages are involved in the pathogenic mechanism of DR. In this study, we further investigated the effects of KL, an anti-aging protein, on senescent macrophages, focusing on anti-aging mechanisms.

Type 2 diabetes increases with age; aging is an important risk factor for its development [34]. The diabetic microenvironment leads to the accumulation of senescent cells, which may cause tissue dysfunction and comorbidities [35]. Our results showed that retinal senescence occured in the DM mouse model, which is consistent with previous studies [36]. Macrophage polarization is an important hallmark of DR pathologies [7, 37]. Macrophages can be polarized to dual-function phenotypes ranging from M1 (pro-inflammatory) to M2 (anti-inflammatory) phenotype [38]. However, macrophages observed in aged mice bear typical M2 marker proteins but simultaneously express a pro-inflammatory factor profile [12, 13], which may be a unique phenotypic alteration characteristic of aging macrophages [39, 40]. We also verified the up-regulation of angiogenic factors (IL-10, TGF-β, CSF2, CSF3, VEGFA, MMP2) and inflammatory factors (TNF-α, IL-1a, CXCL10) in senescent macrophage in Fig. 1. This may explain why the level of intraocular inflammation does not decrease during PDR despite the occurrence of neovascularization and fibrosis (M2 activation) [41, 42]. These complex interactions may lead to "malignant" positive feedback, in which metabolic dysfunction in prediabetes leads to cellular senescence, triggering worsening tissue and metabolic function, further increasing the formation of senescent cells and decreasing the clearance of senescent cells [43]. Therefore, we speculated that a therapy that reduces senescent macrophages may ameliorate DM-induced retinopathy [44, 45].

KL is a well-established longevity protein [46]. Its most prominent function is the regulation of phosphate homeostasis, a hallmark of mammalian aging [47]. However, KL possesses multiple pleiotropic activities, including inhibiting fibrosis, reducing oxidative stress and suppressing inflammation [48–50]. Previous studies have shown that serum KL levels are significantly reduced in diabetes patients [51, 52]. We also found that compared with the Control group, KL levels in the serum, aqueous humor, and vitreous humor were evidently decreased in the PDR group, and 4HNE or palmitic acid also suppressed the expression of KL in RAW264.7 cells. We observed a similar phenomenon in the retinas of diabetic mice. Meanwhile, lower circulating levels of the KL are associated with increased risk of progression of DR [53]. KL has the potential to serve as a promising biomarker for the DR [53]. Our results demonstrate that KL reverses DM-induced retinal senescence and inhibits aging induced by 4HNE in RAW264.7 cells. These results showed that the age-regulating protein KL is vital for sustaining retinal function [54]. Hypoxia-induced VEGF expression has been considered to be a key molecule involved in the pathological increased neoangiogenesis and vascular permeability observed in retinal diseases [55]. Although anti-VEGF agents show remarkably clinical benefits, the costs, the need for frequent intravitreal injections, and the drug resistance have driven interest in studying new treatment targets or additive therapy [56–58]. FGF2 is known as a potent angiogenic factor that is more abundant in macrophages in the hypoxic retina. Aging macrophages trigger the increase in necroptosis [59]. The RIP1-RIP3–mediated

(See figure on next page.)

Fig. 5 KL reverses macrophage senescence in the retina of diabetic mice. **A** SA-β-gal staining and immunofluorescence of anti-P53 (red) antibody in the retina; scale bar = 20 μm ($n = 3$). **B** The fluorescence intensity of P53 was quantified and is displayed in the bar graph (n = 3). **C** Western blotting measured the protein expression level of P21 and P16 in the retina of T2DM + KL group compared to the T2DM group ($n = 3$). **D**, **E** Bar graph showing quantification of P21 and P16 expression in western blot ($n = 3$). **F** Immunofluorescence of anti-F4/80 (red) antibody in the retina; scale bar = 20 μm ($n = 3$). **G** SA-β-gal staining and immunofluorescence of anti-P53 (green) antibody in RAW264.7 cells; scale bar = 50 μm/20 μm ($n = 3$). (H) The fluorescence intensity of P53 was quantified and is displayed in the bar graph ($n = 3$). (I) RAW264.7 cells were further treated with 4HNE after transfection with ADV-GFP or ADV-KL. The expression of P21 and P16 in cells was investigated and quantified ($n = 3$). (J, K) Bar graph showing quantification of P21 and P16 expression in western blot ($n = 3$). (L) Quantification of SASP mRNA expression in RAW264.7 cells ($n = 6$). β-actin was used as control. (M) Immunofluorescence of anti-Ki67 (green) antibody in RAW264.7 cells; scale bar = 20 μm ($n = 3$). (N) Proportions of Ki67 positive cells in different groups. (O) Western blotting measured the protein expression level of P53, P21, and P16 in the mouse PBMCs ($n = 3$). (P, Q, R) Bar graph showing quantification of P53, P21, and P16 expression ($n = 3$). Data represent the mean ± SEM. $*p < 0.05$, $**p < 0.01$, $***p < 0.001$, $****p < 0.0001$, by independent samples t-test

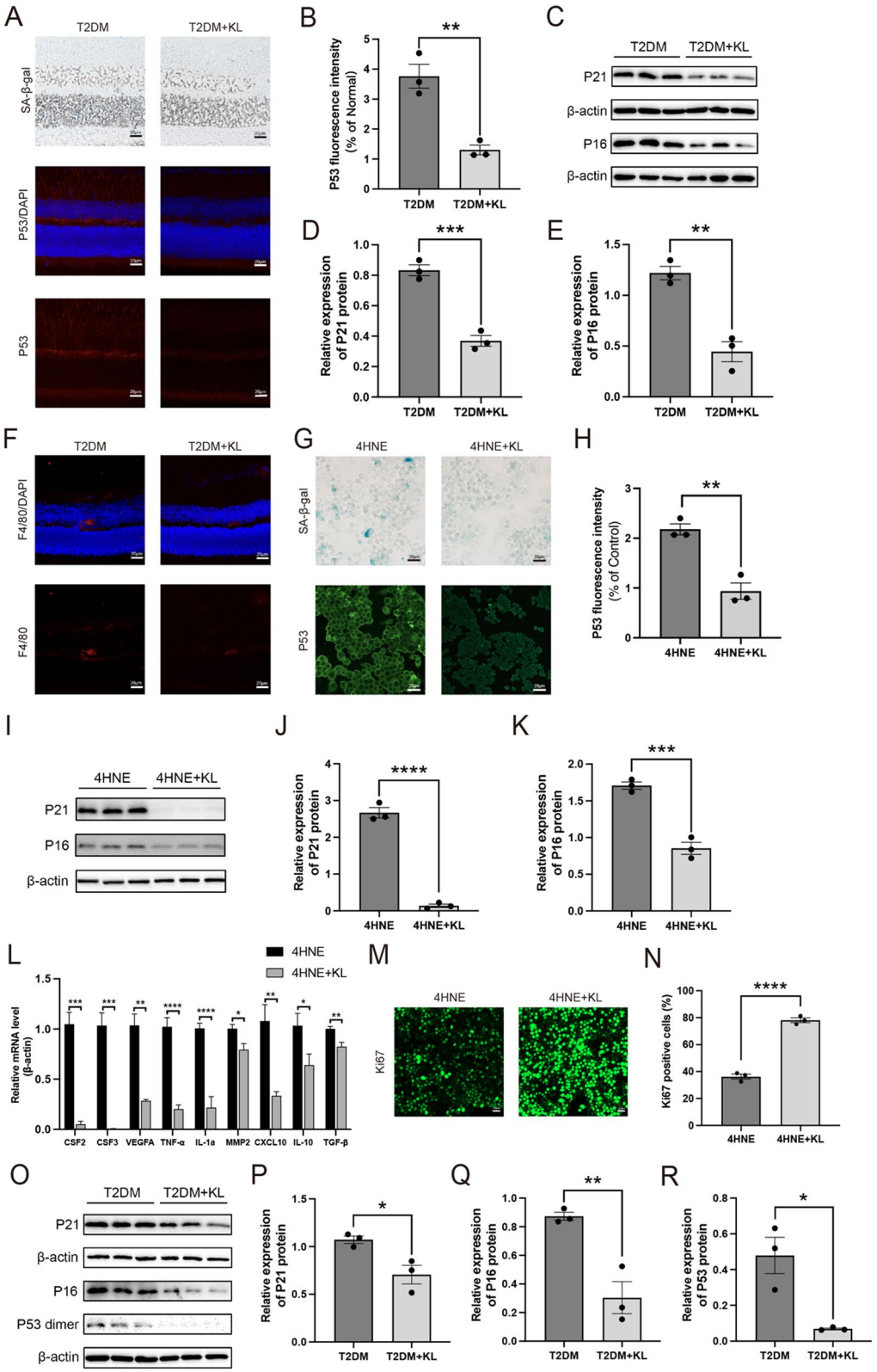

Fig. 5 (See legend on previous page.)

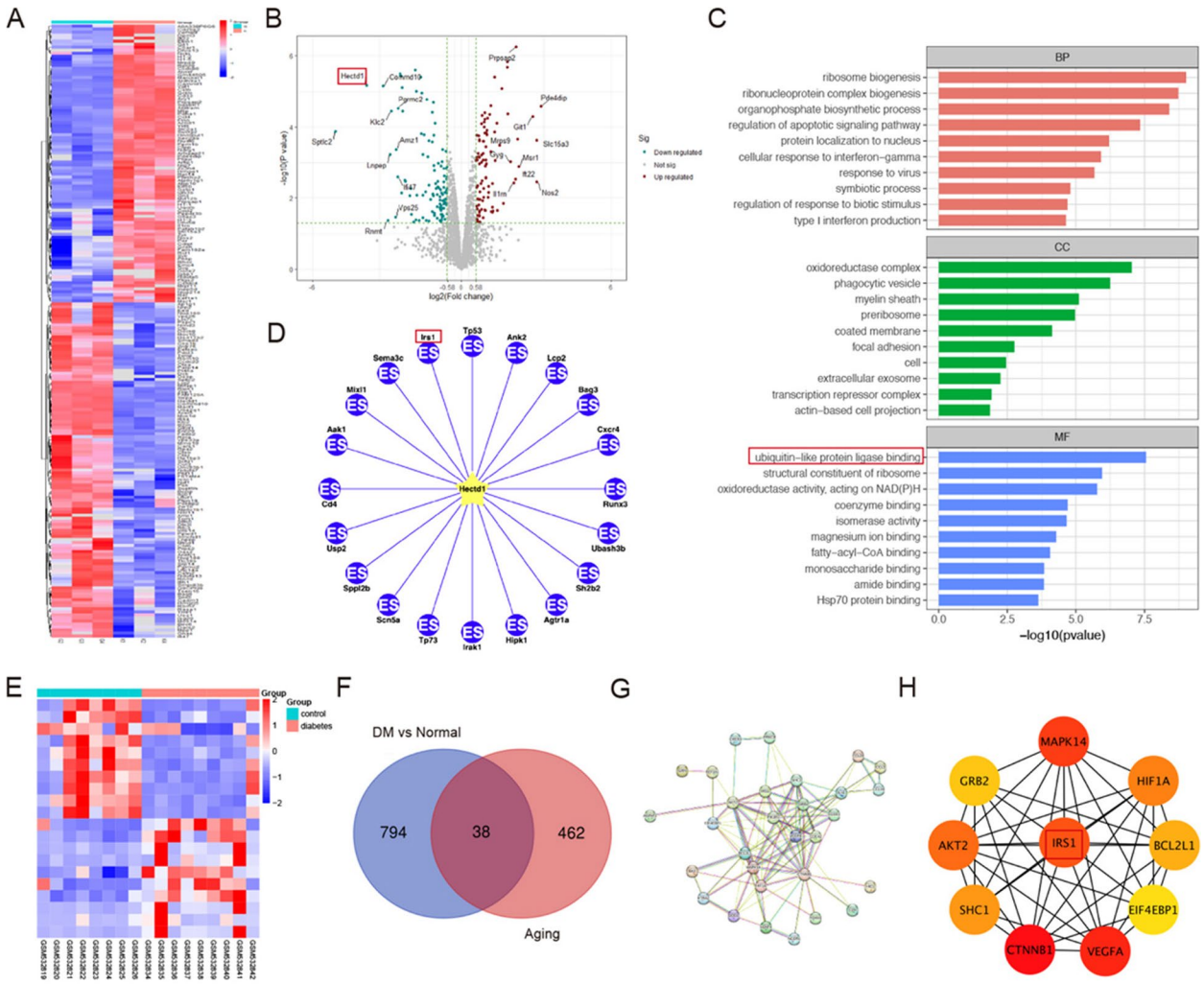

Fig. 6 Exploration of the mechanism of anti-senescence activity of KL. **A** Heatmap showing the DEPs in RAW264.7 cells with or without Ad-KL transfection. **B** Volcanic plot displaying the DEPs in RAW264.7 cells with or without Ad-KL transfection. **C** GO pathway analyses were employed to determine the biofunctions and associated signal paths for DEPs. **D** Top 10 E3 ligase substrates of HECTD1. **E** Heatmap showing the Top 10 DEGs in the GSE26168 datasets. **F** Venn diagrams showing common DEGs in DM and aging. **G** The PPI between 38 differentially expressed senescence-related genes was constructed using the STRING database. The node represents the gene, and the edge represents the gene relationship. **H** The first 10 genes identified through the maximal clique centrality method were screened as hub genes using the cytoHubba plugin. Increased red color represents more forward ranking

necroptosis induced the production and release of FGF2 from macrophages [60]. We uncovered that KL administration attenuated the neovascular lesions by altering the activation state of macrophages and decreasing the expression of VEGFA and FGF2. This synergistic effects for treating angiogenic retinopathy warrants future clinical validation. Targeting KL with approved drugs may be an effective approach to treat DR. According to current study, biguanides, sodium-glucose co-transporter 2 inhibitors, thiazolidinediones, renin–angiotensin–aldosterone inhibitors, statins, vitamin D supplements, mTOR inhibitor, nonspecific phosphodiesterase inhibitor, and phytotherapeutics have been found to increase KL concentrations, and KL supplementation has not caused any toxic side effects [61–70]. As clinical trials have not been performed to evaluate the efficacy of KL in the treatment of DR, further studies are needed to determine the safety of long-term administration of recombinant KL or KL supplements.

We performed a proteomics analysis of RAW264.7 cells transfected with ADV-KL and revealed the expression profile of proteins in a macrophage model overexpressing

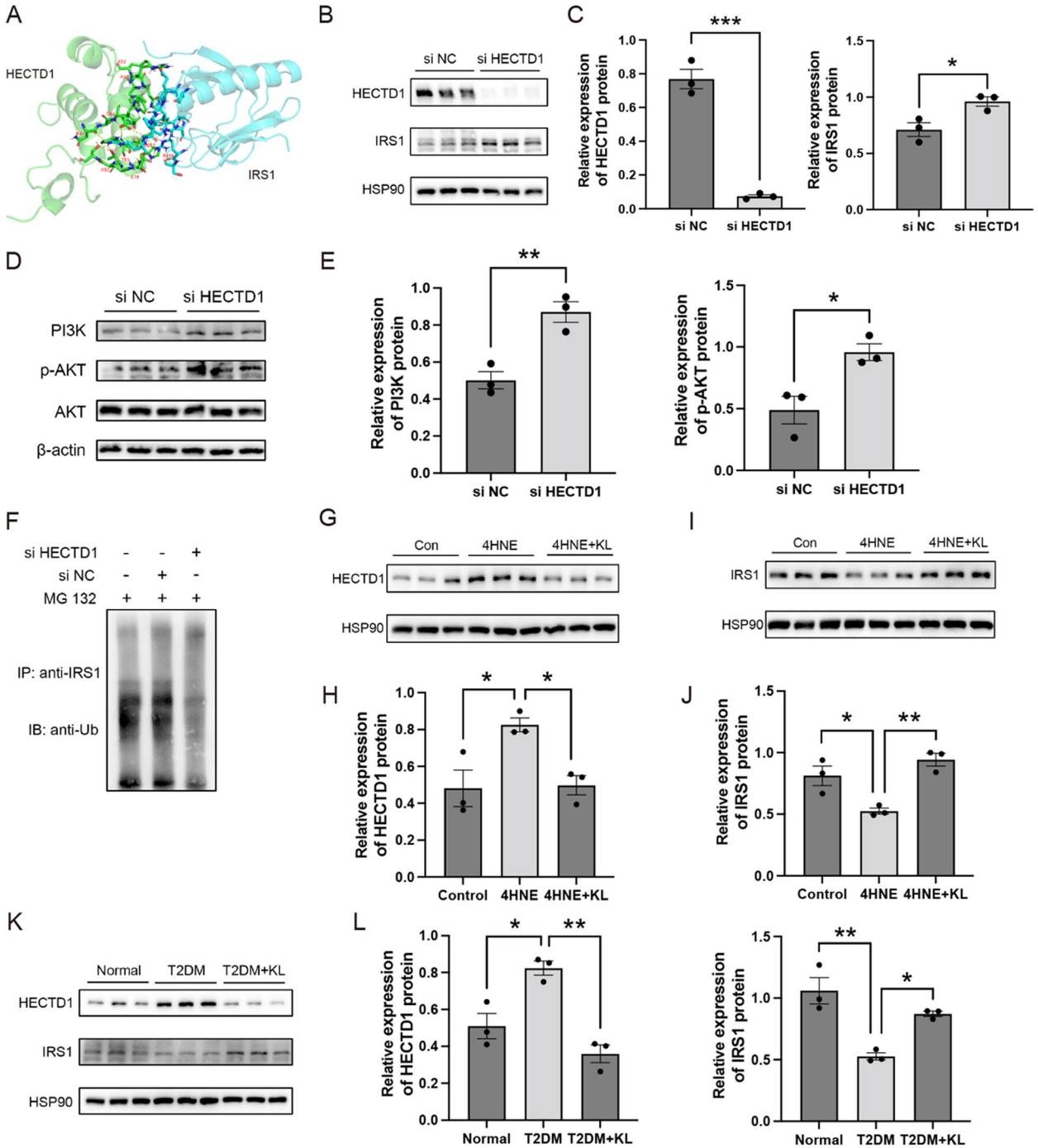

Fig. 7 KL alleviates macrophage senescence by downregulating HECTD1 to decrease IRS1 ubiquitination and degradation. **A** Molecular docking complexes of the HECTD1 solution NMR structure (green) and IRS1 PTB domain (blue) as obtained from ClusPro 2.0. The images were prepared using PyMOL. **B**, **C** RAW264.7 cells were transfected with HECTD1-siRNA for 72 h, followed by western blotting with anti-HECTD1 and anti-IRS1. The expression of HECTD1 and IRS1 in cells was investigated and quantified ($n = 3$). **D**, **E** The expression of PI3K, p-AKT and AKT in cells was investigated and quantified ($n = 3$). **F** RAW264.7 cells were transfected with HECTD1-siRNA for 72 h, followed by immunoprecipitation with anti-IRS1 and immunoblotting with anti-ubiquitin (anti-Ub). **G**-**J** RAW264.7 cells were further treated with 4HNE after transfection with ADV-GFP or ADV-KL. The expression of HECTD1 and IRS1 in cells was investigated and quantified ($n = 3$). **K**, **L** The effects of KL on HECTD1 and IRS1 levels were observed by Western blot in the mouse PBMCs. Data represent the mean ± SEM. $*p < 0.05$, $**p < 0.01$, $***p < 0.001$, by independent samples t-test and one-way ANOVA

KL, which showed 111 upregulated and 92 down-regulated proteins. Based on a bioinformatics analysis, HECTD1 attracted our attention because HECTD1 is an E3 ubiquitin ligase that tags proteins for proteasomal degradation [71]. Interestingly, HECTD1 regulates macrophage polarization, fibroblast migration, and or proliferation by ubiquitinating key proteins [72, 73]. IRS1, a potential ubiquitination substrate of HECTD1, is a key molecule involved in insulin signal transmission and plays a key role in insulin resistance [74]. Carvalho et al. [75] reported that individuals with T2DM and those at risk of developing diabetes could be identified via reduced IRS1 mRNA and protein levels. Hyperglycemia induces a decrease in the protein level of IRS1 in retinal endothelial cells [76]. Rescue of IRS1 may decrease retinal endothelial cell apoptosis and potentially improve diabetic retinopathy outcomes [77].

There are some limitations to the current study. First, we only demonstrated the therapeutic effect of KL in T1DM mice; however, the underlying mechanism was not explored. Second, we only discussed the HECTD1/IRS1 signaling pathway; the other pathways were unclear. Third, the ubiquitination of IRS1 should also be further investigated in DR.

Conclusion

In summary, this study demonstrated the protective role of KL in DR. In addition, we uncovered a novel mechanism associated with the protective effect of KL against DM-induced retinal macrophage senescence. Therefore, we recommend that modulation of KL expression is an exciting and viable target for DR. Our report provides new insights into the mechanisms of DR and may lead to the development of future therapeutics to diminish its burden.

Abbreviations

4HNE	4-Hydroxynonenal
Ad	Adenovirus
DEPs	Differentially expressed proteins
DIA	Data Independent Acquisition
DM	Diabetes mellitus
ELISA	Enzyme-Linked Immunosorbent assay
ERG	Electroretinography
GO	Gene ontology
HFD	High-fat diet
KL	α-Klotho
NPDR	Non-proliferative diabetic retinopathy
OCT	Optical Coherence Tomography
PBMCs	Peripheral Blood Mononuclear Cells
PDR	Proliferative diabetic retinopathy
PPI	Protein–protein interaction
qRT-PCR	Quantitative Real-Time Polymerase Chain Reaction
SASP	Senescence-associated secretory phenotype
STRING	Search Tool for the Retrieval of Interacting Genes
STZ	Streptozotocin

Supplementary Information

The online version contains supplementary material available at https://doi.org/10.1186/s12964-024-01838-w.

Supplementary Material 1.

Authors' contributions

Qingbo Li (first author): Writing - Original Draft, Data Curation, Investigation. Peiyu Wang: Resources, Validation. Yi Gong: Resources. Manhong Xu: Resources. Manqiao Wang: Resources. Rong Luan: Resources. Juping Liu (corresponding author): Methodology, Supervision. Xiaorong Li (corresponding author): Conceptualization, Methodology, Supervision. Yan Shao (corresponding author): Conceptualization, Methodology, Supervision, Writing - Review & Editing.

Funding

This work was supported by grants from the project of central government supports for Tibet development (XZ202301YD0029C), and National Natural Science Foundation of China (82360209).

Availability of data and materials

No datasets were generated or analysed during the current study.

Declarations

Competing interests

The authors declare no competing interests.

Author details

[1]Tianjin Key Laboratory of Retinal Functions and Diseases, Eye Institute & School of Optometry and Ophthalmology, Tianjin Medical University Eye Hospital, Nankai District, No. 251, Fukang Road, Tianjin 300384, China. [2]Tianjin International Joint Research and Development Centre of Ophthalmology and Vision Science, Tianjin Medical University Eye Hospital, Nankai District, No. 251, Fukang Road, Tianjin 300384, China. [3]Eye Institute and School of Optometry, Tianjin Medical University Eye Hospital, Nankai District, No. 251, Fukang Road, Tianjin 300384, China. [4]University of Tibetan Medicine, Lhasa 850000, China.

Received: 9 July 2024 Accepted: 18 September 2024
Published online: 26 September 2024

References

1. Cho NH, Shaw JE, Karuranga S, Huang Y, da Rocha Fernandes JD, Ohlrogge AW, Malanda B. IDF Diabetes Atlas: Global estimates of diabetes prevalence for 2017 and projections for 2045. Diabetes Res Clin Pract. 2018;138:271–81.
2. Tarr JM, Kaul K, Chopra M, Kohner EM, Chibber R. Pathophysiology of diabetic retinopathy ISRN Ophthalmol. 2013;2013: 343560.
3. Romero-Aroca P, Navarro-Gil R, Valls-Mateu A, Sagarra-Alamo R, Moreno-Ribas A, Soler N. Differences in incidence of diabetic retinopathy between type 1 and 2 diabetes mellitus: a nine-year follow-up study. Br J Ophthalmol. 2017;101:1346–51.
4. Li Q, Wang M, Li X, Shao Y. Aging and diabetic retinopathy: Inherently intertwined pathophysiological processes. Exp Gerontol. 2023;175: 112138.
5. Kang Q, Yang C. Oxidative stress and diabetic retinopathy: Molecular mechanisms, pathogenetic role and therapeutic implications. Redox Biol. 2020;37: 101799.
6. Chen Q, Fischer A, Reagan JD, Yan LJ, Ames BN. Oxidative DNA damage and senescence of human diploid fibroblast cells. Proc Natl Acad Sci U S A. 1995;92:4337–41.
7. Kinuthia UM, Wolf A, Langmann T. Microglia and Inflammatory Responses in Diabetic Retinopathy. Front Immunol. 2020;11: 564077.

8. Wu H, Wang M, Li X, Shao Y. The Metaflammatory and Immunometabolic Role of Macrophages and Microglia in Diabetic Retinopathy. Hum Cell. 2021;34:1617–28.
9. Shapouri-Moghaddam A, Mohammadian S, Vazini H, Taghadosi M, Esmaeili SA, Mardani F, Seifi B, Mohammadi A, Afshari JT, Sahebkar A. Macrophage plasticity, polarization, and function in health and disease. J Cell Physiol. 2018;233:6425–40.
10. Liu Z, Xu J, Ma Q, Zhang X, Yang Q, Wang L, Cao Y, Xu Z, Tawfik A, Sun Y, et al: Glycolysis links reciprocal activation of myeloid cells and endothelial cells in the retinal angiogenic niche. Sci Transl Med 2020, 12.
11. Behmoaras J, Gil J: Similarities and interplay between senescent cells and macrophages. J Cell Biol 2021, 220.
12. Hall BM, Balan V, Gleiberman AS, Strom E, Krasnov P, Virtuoso LP, Rydkina E, Vujcic S, Balan K, Gitlin I, et al. Aging of mice is associated with p16(Ink4a)- and β-galactosidase-positive macrophage accumulation that can be induced in young mice by senescent cells. Aging (Albany NY). 2016;8:1294–315.
13. Hall BM, Balan V, Gleiberman AS, Strom E, Krasnov P, Virtuoso LP, Rydkina E, Vujcic S, Balan K, Gitlin II, et al. p16(Ink4a) and senescence-associated β-galactosidase can be induced in macrophages as part of a reversible response to physiological stimuli. Aging (Albany NY). 2017;9:1867–84.
14. Nabeshima Y. Klotho: a fundamental regulator of aging. Ageing Res Rev. 2002;1:627–38.
15. Lin Y, Sun Z. Antiaging Gene Klotho Attenuates Pancreatic β-Cell Apoptosis in Type 1 Diabetes. Diabetes. 2015;64:4298–311.
16. Jiang W, Gan C, Zhou X, Yang Q, Chen D, Xiao H, Dai L, Chen Y, Wang M, Yang H, Li Q. Klotho inhibits renal ox-LDL deposition via IGF-1R/RAC1/OLR1 signaling to ameliorate podocyte injury in diabetic kidney disease. Cardiovasc Diabetol. 2023;22:293.
17. Typiak M, Piwkowska A: Antiinflammatory Actions of Klotho: Implications for Therapy of Diabetic Nephropathy. Int J Mol Sci 2021, 22.
18. Ji B, Wei H, Ding Y, Liang H, Yao L, Wang H, Qu H, Deng H. Protective potential of klotho protein on diabetic retinopathy: Evidence from clinical and in vitro studies. J Diabetes Investig. 2020;11:162–9.
19. Dham D, Roy B, Gowda A, Pan G, Sridhar A, Zeng X, Thandavarayan RA, Palaniyandi SS. 4-Hydroxy-2-nonenal, a lipid peroxidation product, as a biomarker in diabetes and its complications: challenges and opportunities. Free Radic Res. 2021;55:547–61.
20. Zhou T, Zhou KK, Lee K, Gao G, Lyons TJ, Kowluru R, Ma JX. The role of lipid peroxidation products and oxidative stress in activation of the canonical wingless-type MMTV integration site (WNT) pathway in a rat model of diabetic retinopathy. Diabetologia. 2011;54:459–68.
21. Sarac O, Gulsuner S, Yildiz-Tasci Y, Ozcelik T, Kansu T. Neuro-ophthalmologic findings in humans with quadrupedal locomotion. Ophthalmic Genet. 2012;33:249–52.
22. Joyal JS, Sun Y, Gantner ML, Shao Z, Evans LP, Saba N, Fredrick T, Burnim S, Kim JS, Patel G, et al. Retinal lipid and glucose metabolism dictates angiogenesis through the lipid sensor Ffar1. Nat Med. 2016;22:439–45.
23. Yanagi Y, Foo VHX, Yoshida A. Asian age-related macular degeneration: from basic science research perspective. Eye (Lond). 2019;33:34–49.
24. Kano MR, Morishita Y, Iwata C, Iwasaka S, Watabe T, Ouchi Y, Miyazono K, Miyazawa K. VEGF-A and FGF-2 synergistically promote neoangiogenesis through enhancement of endogenous PDGF-B-PDGFRbeta signaling. J Cell Sci. 2005;118:3759–68.
25. Min J, Zeng T, Roux M, Lazar D, Chen L, Tudzarova S. The Role of HIF1α-PFKFB3 Pathway in Diabetic Retinopathy. J Clin Endocrinol Metab. 2021;106:2505–19.
26. Kowluru RA, Tang J, Kern TS: Abnormalities of retinal metabolism in diabetes and experimental galactosemia. VII. Effect of long-term administration of antioxidants on the development of retinopathy. Diabetes 2001, 50:1938–1942.
27. Zhong Y, Li J, Chen Y, Wang JJ, Ratan R, Zhang SX. Activation of endoplasmic reticulum stress by hyperglycemia is essential for Müller cell-derived inflammatory cytokine production in diabetes. Diabetes. 2012;61:492–504.
28. Cetin EN, Bulgu Y, Ozdemir S, Topsakal S, Akın F, Aybek H, Yıldırım C. Association of serum lipid levels with diabetic retinopathy. Int J Ophthalmol. 2013;6:346–9.
29. Shi H, Zhang Z, Wang X, Li R, Hou W, Bi W, Zhang X. Inhibition of autophagy induces IL-1β release from ARPE-19 cells via ROS mediated NLRP3 inflammasome activation under high glucose stress. Biochem Biophys Res Commun. 2015;463:1071–6.
30. Ahmed W, Lingner J. Impact of oxidative stress on telomere biology. Differentiation. 2018;99:21–7.
31. Pluquet O, Pourtier A, Abbadie C: The unfolded protein response and cellular senescence. A review in the theme: cellular mechanisms of endoplasmic reticulum stress signaling in health and disease. Am J Physiol Cell Physiol 2015, 308:C415–425.
32. Newsholme P, de Bittencourt PI, Jr. The fat cell senescence hypothesis: a mechanism responsible for abrogating the resolution of inflammation in chronic disease. Curr Opin Clin Nutr Metab Care. 2014;17:295–305.
33. Kroemer G. Autophagy: a druggable process that is deregulated in aging and human disease. J Clin Invest. 2015;125:1–4.
34. Sun P, Wen H, Liu X, Ma Y, Jang J, Yu C. Time trends in type 2 diabetes mellitus incidence across the BRICS from 1990 to 2019: an age-period-cohort analysis. BMC Public Health. 2022;22:65.
35. Palmer AK, Tchkonia T, LeBrasseur NK, Chini EN, Xu M, Kirkland JL. Cellular Senescence in Type 2 Diabetes: A Therapeutic Opportunity. Diabetes. 2015;64:2289–98.
36. Crespo-Garcia S, Tsuruda PR, Dejda A, Ryan RD, Fournier F, Chaney SY, Pilon F, Dogan T, Cagnone G, Patel P, et al. Pathological angiogenesis in retinopathy engages cellular senescence and is amenable to therapeutic elimination via BCL-xL inhibition. Cell Metab. 2021;33:818–832.e817.
37. Li J, Yu S, Lu X, Cui K, Tang X, Xu Y, Liang X. The phase changes of M1/M2 phenotype of microglia/macrophage following oxygen-induced retinopathy in mice. Inflamm Res. 2021;70:183–92.
38. Locati M, Curtale G, Mantovani A. Diversity, Mechanisms, and Significance of Macrophage Plasticity. Annu Rev Pathol. 2020;15:123–47.
39. van Beek AA, Van den Bossche J, Mastroberardino PG, de Winther MPJ, Leenen PJM. Metabolic Alterations in Aging Macrophages: Ingredients for Inflammaging? Trends Immunol. 2019;40:113–27.
40. Schädel P, Czapka A, Gebert N, Jacobsen ID, Ori A, Werz O. Metabololipidomic and proteomic profiling reveals aberrant macrophage activation and interrelated immunomodulatory mediator release during aging. Aging Cell. 2023;22: e13856.
41. Wu F, Phone A, Lamy R, Ma D, Laotaweerungsawat S, Chen Y, Zhao T, Ma W, Zhang F, Psaras C, Stewart JM. Correlation of Aqueous, Vitreous, and Plasma Cytokine Levels in Patients With Proliferative Diabetic Retinopathy. Invest Ophthalmol Vis Sci. 2020;61:26.
42. Feng S, Yu H, Yu Y, Geng Y, Li D, Yang C, Lv Q, Lu L, Liu T, Li G, Yuan L. Levels of Inflammatory Cytokines IL-1β, IL-6, IL-8, IL-17A, and TNF-α in Aqueous Humour of Patients with Diabetic Retinopathy. J Diabetes Res. 2018;2018:8546423.
43. Nelson G, Wordsworth J, Wang C, Jurk D, Lawless C, Martin-Ruiz C, von Zglinicki T. A senescent cell bystander effect: senescence-induced senescence. Aging Cell. 2012;11:345–9.
44. Kirkland JL, Tchkonia T. Clinical strategies and animal models for developing senolytic agents. Exp Gerontol. 2015;68:19–25.
45. Minhas PS, Latif-Hernandez A, McReynolds MR, Durairaj AS, Wang Q, Rubin A, Joshi AU, He JQ, Gauba E, Liu L, et al. Restoring metabolism of myeloid cells reverses cognitive decline in ageing. Nature. 2021;590:122–8.
46. Kurosu H, Yamamoto M, Clark JD, Pastor JV, Nandi A, Gurnani P, McGuinness OP, Chikuda H, Yamaguchi M, Kawaguchi H, et al. Suppression of aging in mice by the hormone Klotho. Science. 2005;309:1829–33.
47. Buchanan S, Combet E, Stenvinkel P, Shiels PG. Klotho, Aging, and the Failing Kidney. Front Endocrinol (Lausanne). 2020;11:560.
48. Ligumsky H, Merenbakh-Lamin K, Keren-Khadmy N, Wolf I, Rubinek T. The role of α-klotho in human cancer: molecular and clinical aspects. Oncogene. 2022;41:4487–97.
49. Xie L, Wang Y, Li Q, Ji X, Tu Y, Du S, Lou H, Zeng X, Zhu L, Zhang J, Zhu M. The HIF-1α/p53/miRNA-34a/Klotho axis in retinal pigment epithelial cells promotes subretinal fibrosis and exacerbates choroidal neovascularization. J Cell Mol Med. 2021;25:1700–11.
50. Yuan Q, Ren Q, Li L, Tan H, Lu M, Tian Y, Huang L, Zhao B, Fu H, Hou FF, et al. A Klotho-derived peptide protects against kidney fibrosis by targeting TGF-β signaling. Nat Commun. 2022;13:438.
51. Nie F, Wu D, Du H, Yang X, Yang M, Pang X, Xu Y. Serum klotho protein levels and their correlations with the progression of type 2 diabetes mellitus. J Diabetes Complications. 2017;31:594–8.

52. Tarhani F, Heidari G, Nezami A. Evaluation of α-klotho level in insulin dependent diabetes mellitus (IDDM) children. J Pediatr Endocrinol Metab. 2020;33:761–5.
53. Corcillo A, Fountoulakis N, Sohal A, Farrow F, Ayis S, Karalliedde J. Low levels of circulating anti-ageing hormone Klotho predict the onset and progression of diabetic retinopathy. Diab Vasc Dis Res. 2020;17:1479164120970901.
54. Reish NJ, Maltare A, McKeown AS, Laszczyk AM, Kraft TW, Gross AK, King GD. The age-regulating protein klotho is vital to sustain retinal function. Invest Ophthalmol Vis Sci. 2013;54:6675–85.
55. Campochiaro PA. Molecular pathogenesis of retinal and choroidal vascular diseases. Prog Retin Eye Res. 2015;49:67–81.
56. Ferro Desideri L, Barra F, Ferrero S, Traverso CE, Nicolò M. Clinical efficacy and safety of ranibizumab in the treatment of wet age-related macular degeneration. Expert Opin Biol Ther. 2019;19:735–51.
57. Ferro Desideri L, Traverso CE, Nicolò M. Abicipar pegol: an investigational anti-VEGF agent for the treatment of wet age-related macular degeneration. Expert Opin Investig Drugs. 2020;29:651–8.
58. Nicolò M, Ferro Desideri L, Vagge A, Traverso CE. Faricimab: an investigational agent targeting the Tie-2/angiopoietin pathway and VEGF-A for the treatment of retinal diseases. Expert Opin Investig Drugs. 2021;30:193–200.
59. Royce GH, Brown-Borg HM, Deepa SS. The potential role of necroptosis in inflammaging and aging. Geroscience. 2019;41:795–811.
60. He C, Liu Y, Huang Z, Yang Z, Zhou T, Liu S, Hao Z, Wang J, Feng Q, Liu Y, et al: A specific RIP3(+) subpopulation of microglia promotes retinopathy through a hypoxia-triggered necroptotic mechanism. Proc Natl Acad Sci U S A 2021, 118.
61. Tang A, Zhang Y, Wu L, Lin Y, Lv L, Zhao L, Xu B, Huang Y, Li M. Klotho's impact on diabetic nephropathy and its emerging connection to diabetic retinopathy. Front Endocrinol (Lausanne). 2023;14:1180169.
62. Yoon HE, Lim SW, Piao SG, Song JH, Kim J, Yang CW. Statin upregulates the expression of klotho, an anti-aging gene, in experimental cyclosporine nephropathy. Nephron Exp Nephrol. 2012;120:e123–133.
63. Mora-Fernández C, Sánchez-Niño MD, Donate-Correa J, Martín-Núñez E, Pérez-Delgado N, Valiño-Rivas L, Fernández-Fernández B, Ortiz A, Navarro-González JF. Sodium-glucose co-transporter-2 inhibitors increase Klotho in patients with diabetic kidney disease: A clinical and experimental study. Biomed Pharmacother. 2022;154: 113677.
64. Karalliedde J, Maltese G, Hill B, Viberti G, Gnudi L. Effect of renin-angiotensin system blockade on soluble Klotho in patients with type 2 diabetes, systolic hypertension, and albuminuria. Clin J Am Soc Nephrol. 2013;8:1899–905.
65. Xue J, Wang L, Sun Z, Xing C. Basic Research in Diabetic Nephropathy Health Care: A study of the Renoprotective Mechanism of Metformin. J Med Syst. 2019;43:266.
66. Zhang H, Li Y, Fan Y, Wu J, Zhao B, Guan Y, Chien S, Wang N. Klotho is a target gene of PPAR-gamma. Kidney Int. 2008;74:732–9.
67. Lerch C, Shroff R, Wan M, Rees L, Aitkenhead H, Kaplan Bulut I, Thurn D, Karabay Bayazit A, Niemirska A, Canpolat N, et al. Effects of nutritional vitamin D supplementation on markers of bone and mineral metabolism in children with chronic kidney disease. Nephrol Dial Transplant. 2018;33:2208–17.
68. Zhao Y, Zhao MM, Cai Y, Zheng MF, Sun WL, Zhang SY, Kong W, Gu J, Wang X, Xu MJ. Mammalian target of rapamycin signaling inhibition ameliorates vascular calcification via Klotho upregulation. Kidney Int. 2015;88:711–21.
69. Navarro-González JF, Sánchez-Niño MD, Donate-Correa J, Martín-Núñez E, Ferri C, Pérez-Delgado N, Górriz JL, Martínez-Castelao A, Ortiz A, Mora-Fernández C. Effects of Pentoxifylline on Soluble Klotho Concentrations and Renal Tubular Cell Expression in Diabetic Kidney Disease. Diabetes Care. 2018;41:1817–20.
70. Castillo RF. Pathophysiologic Implications and Therapeutic Approach of Klotho in Chronic Kidney Disease: A Systematic Review. Lab Invest. 2023;103: 100178.
71. Shaid S, Brandts CH, Serve H, Dikic I. Ubiquitination and selective autophagy. Cell Death Differ. 2013;20:21–30.
72. Deng S, Huang C. E3 ubiquitin ligases in regulating stress fiber, lamellipodium, and focal adhesion dynamics. Cell Adh Migr. 2014;8:49–54.
73. Zhou Z, Jiang R, Yang X, Guo H, Fang S, Zhang Y, Cheng Y, Wang J, Yao H, Chao J. circRNA Mediates Silica-Induced Macrophage Activation Via HECTD1/ZC3H12A-Dependent Ubiquitination. Theranostics. 2018;8:575–92.
74. White MF. IRS proteins and the common path to diabetes. Am J Physiol Endocrinol Metab. 2002;283:E413–422.
75. Carvalho E, Jansson PA, Axelsen M, Eriksson JW, Huang X, Groop L, Rondinone C, Sjöström L, Smith U. Low cellular IRS 1 gene and protein expression predict insulin resistance and NIDDM. Faseb j. 1999;13:2173–8.
76. Jiang Y, Biswas SK, Steinle JJ. Serine 307 on insulin receptor substrate 1 is required for SOCS3 and TNF-α signaling in the rMC-1 cell line. Mol Vis. 2014;20:1463–70.
77. Lavin DP, White MF, Brazil DP. IRS proteins and diabetic complications. Diabetologia. 2016;59:2280–91.

Publisher's Note

Springer Nature remains neutral with regard to jurisdictional claims in published maps and institutional affiliations.